Double lateral antiresonant structures

Fig 5.10: Near field images of the ARROW-2D waveguides with double lateral antiresonant structures.

It has been observed that using the ARROW-2D configuration, it is possible to obtain large core waveguides (≤20μm) with single-mode behavior. Double lateral antiresonant pairs are able to confine light on waveguides with a width thinner or equal to 10 μm. On the contrary, as it was observed in simulations done in chapter 4, single lateral antiresonant structures does not have so strong confinement properties and the fundamental mode was not seen in waveguides thinner than 16 μm.

5.4 Directional Couplers

5.4.1 Rib Directional Couplers

Between the two antiresonant configurations available, ARROW-B was chosen to obtain rib directional couplers due to its slight minor coupling length as compared to its counterpart based on ARROW-A. This reason is not strong enough so as to reject the latter structures for evanescent-field based devices. Probably, results shown in this subsection would be very similar in case of using these structures.

Fabrication steps are equivalent to those presented in the fabrication of the rib waveguides and for simplicity, the photolithographic step is the only one shown in table 5.4, where a new mask is used. However, the refractive index obtained for the second cladding layer and the core was slightly lower value (n=1.54), while the refractive index value of the first cladding remain unchanged. Reasons for the decrease in the refractive index value could be associated to a variation of the partial pressure of the precursor gases on the reactor during the film deposition. Concretely, a slight increase of the gas flow ratio could lower the refractive index from the expected 1.56 to the obtained refractive index value. From the results shown in section 5.3.1, it can be easily concluded that directional couplers with this waveguide configuration will have higher losses than the previously measured ARROW-B waveguides. Nevertheless, its periodic power exchange between the waveguides should still be obtained.

Mask employed for the directional coupler characterization consists on ten structures, each one with a different length, from 1 to 10mm, at which waveguides are parallel. The rest of the parameters have been chosen in according to the optimization done in chapter 4.
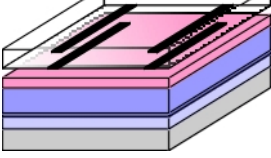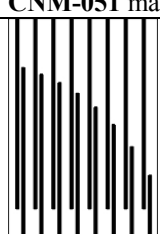
Scheme	Step properties
	CNM-051 mask
	Mask **Parallel length:** 1-10mm in steps of 1mm **Waveguide width:** 5μm **Separation between waveguides:** 2μm **Step:** 2μm positive photoresist

Table 5.4: Photolithographic step for ARROW-B directional couplers fabrication.

Simulation of the directional coupler when a 4μm Gaussian beam is injected in input waveguide can be observed in fig. 5.11, with a coupling length L_c=2052μm. Integration of this latter values allows obtaining the power as a function of the propagation length, shown in fig. 5.12, together with the experimental data measured.
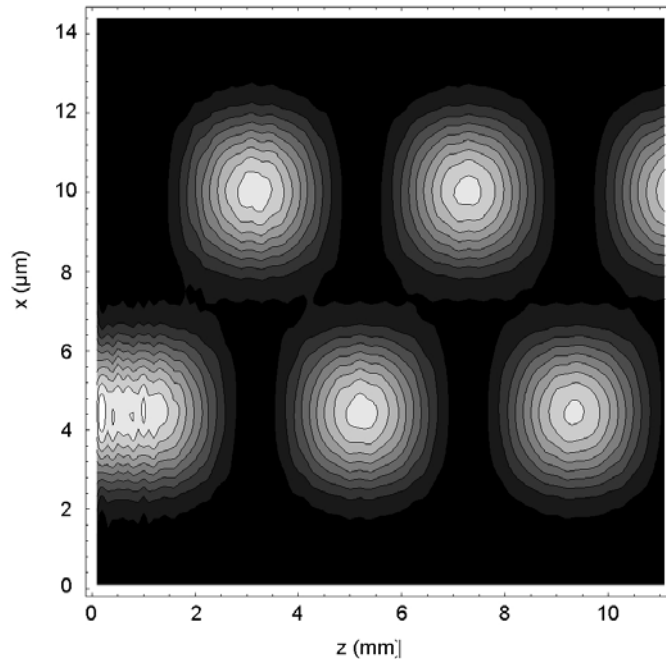

Fig 5.11: NU-FDM/BPM simulation of the directional coupler based on ARROW-B structures, with a Gaussian beam excitation.

It can be observed in figure 5.12 how a nearly complete periodic power exchange is obtained, with a progressively decrease of its magnitude due to the waveguide attenuation. The fact that this exchange is of nearly all the power can be associated to the fact that waveguides are nearly equal and that clean room fabrication steps have been done accordingly to the requested parameters. However, when experimental results are compared to simulations, it can be observed how there exists a

significant mismatch. Several factors could lead to variations in the coupling length, as could be a higher rib, a larger separation between waveguides or slightly wider waveguides. From the previously mentioned assumptions, the former is not feasible, since the directional coupler has been defined in a photolithographic mask and, at utmost, waveguides could be slightly smaller, due to overetching. As far as rib is concerned, measurements done by profilometry showed a rib of $1.53 \pm 0.02\mu m$, which is slightly higher as compared to the theoretical, but not so high as to cause high variations on the coupling length. What was observed during measurements was that waveguide walls where not perfectly vertical, but had a certain tilt, as observed in SEM picture shown in fig 5.13. This variation on the device morphology causes a decrease in the confinement on the waveguides and, as it was described in chapter 4, causes a enhancement of the evanescent field coupling, decreasing the coupling length. Measurements done of the wall tilt showed that it has a 80º angle. This modification was introduced in the simulations and a new coupling length of $1848\mu m$ was obtained, that is in much agreement with the experimental results.
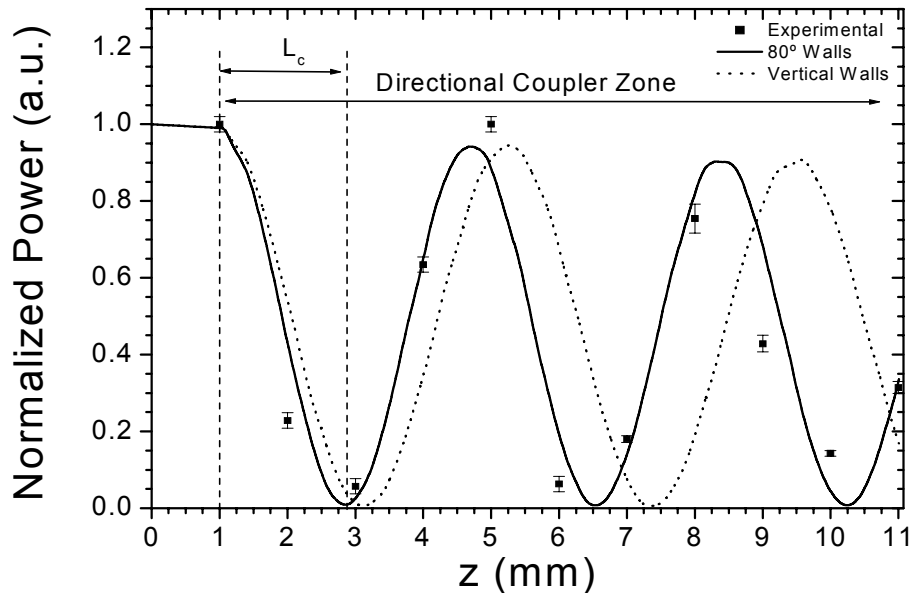
Fig 5.12: Power interchange between ARROW-B waveguides of the Directional Coupler as a function of the distance: Experimental, Simulation with vertical rib and Simulation with 80º tilted rib.
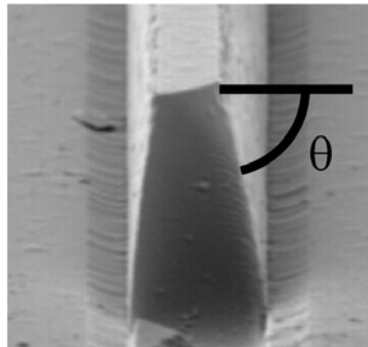
Fig 5.13: 80º Wall tilt on waveguides due to RIE process.

Finally, directional couplers where measured as a function of the wavelength. With the help of the expressions from chapter 2, it can be seen that, for identical waveguides, power exchange only depends on the coupling constant between the evanescent fields. If waveguides are parallel, as are those of the directional coupler presented, the coupling constant does not depend on the propagation constant, that is, it has a constant value. Then, its value only depends on the working wavelength. Thus, since the power transfer has a trigonometric expression, for a fixed length, namely 5000µm, a periodic exchange of power should be obtained at the power output as a function of the working wavelength. Results obtained for the total losses as a function of the wavelength are shown in fig. 5.14.
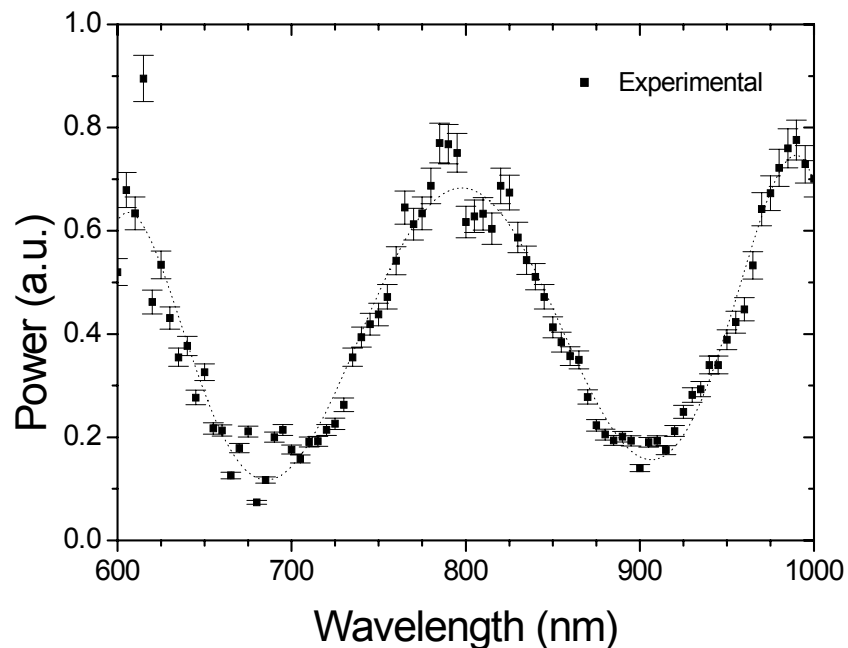

Fig 5.14: Power vs. Wavelength for an ARROW-B directional coupler with L=5000µm.